Electronic Supplementary Material (ESI) for Physical Chemistry Chemical Physics.
This journal is © the Owner Societies 2019

Solvation of Zn^{2+} ion in 1-alkyl-3-methylimidazolium *bis*(trifluoromethylsulfonyl)imide ionic liquids: a molecular dynamics and X-ray absorption study

Matteo Busato,[a] Paola D'Angelo[b] and Andrea Melchior[a*]

[a]DPIA, Laboratorio di Scienze e Tecnologie Chimiche, Università di Udine, Via del Cotonificio 108, 33100 Udine, Italy

[b]Dipartimento di Chimica, Università di Roma "La Sapienza", P.le A. Moro 5, 00185 Roma, Italy

Supporting Information

1. *Evaluation of the RTILs force field and Zn^{2+} Lennard-Jones parameters*

Molecular dynamics simulations (MD) are among the most useful techniques in the study of condensed phases and in particular of ionic liquids. However, the choice of the force field representing the simulated species is not trivial and can have a crucial influence on the extent of the calculated structural and thermodynamic properties. For this reason, in a preliminary phase of this work a comparative study about the RTILs force fields and Zn^{2+} Lennard-Jones parameters has been carried out. To this purpose, OPLS-AA[1] compatible force fields were employed to represent the simulated species. The non-bonded term of the employed potentials has the usual Lennard-Jones and Coulomb terms:

$$U_{ij}(r_{ij}) = 4\varepsilon_{ij}\left[\left(\frac{\sigma_{ij}}{r_{ij}}\right)^{12} - \left(\frac{\sigma_{ij}}{r_{ij}}\right)^{6}\right] + e^2\frac{q_i q_j}{r_{ij}} \qquad (1)$$

For $[C_4mim][Tf_2N]$, the all-atom non-polarizable force fields by Canongia Lopes and Padua (CL&P),[2–4] Ludwig *et al.* (KPL)[5] and Müller-Plathe *et al.* (MP)[6] have been used. For $[C_2mim][Tf_2N]$, simulations have been performed with CL&P[2–4] and KPL[5] parameter sets. As regards the $[Tf_2N]^-$ coordinating oxygen atom, the tested force fields differ in the Lennard-Jones part, while the point charge for this center is the same (Table S1).

The Lennard-Jones parameters (ε, σ) for Zn^{2+} were taken from Merz *et al.* "CM set" for TIP3P water (Merz),[7] Stote and Karplus (SK),[8] and from those implemented by Merz *et al*. in the AMBER force field (AMBER, Table S1).[9]

Table S1. Non-bonded parameters for Zn^{2+} and the oxygen atom of the $[Tf_2N]^-$ anion taken from the force fields employed in this work.

Atom	Potential	q (e)	σ (Å)	ε (kcal mol^{-1})
Zn^{2+}	Merz[7]	2.00	2.265	0.0033
	SK[8]	2.00	1.949	0.250
	AMBER[9]	2.00	1.960	0.0125
$O(Tf_2N)$	CL&P[2–4]	-0.53	2.96	0.21
	KPL[5]	-0.53	3.46	0.063
	MP[6]	-0.53	3.18	0.21

1.1 *Zn^{2+} solvation structure*

MD simulations of Zn^{2+} in $[C_2mim][Tf_2N]$ and $[C_4mim][Tf_2N]$ employing different force fields for the RTILs and LJ parameters for the metal have been carried out as reported in the main text. The obtained structural parameters for the metal first coordination shell are reported in Table S2. The radial distribution functions (RDFs) of the Zn−$O(Tf_2N)$ pairs (Figure S1) show a first intense peak corresponding to six oxygen atoms with all the tested force fields. In nearly all cases, the integrals of the first peak of the Zn-$N(Tf_2N)$ RDFs show that six nitrogen atoms are also present, thus reporting that each of the coordinating oxygen atoms come from a monodentate $[Tf_2N]^-$ anion giving the octahedral $[Zn(Tf_2N)_6]^{4-}$ unit. The only exception is given by the MP[6] force field for $[C_4mim][Tf_2N]$ in combination with AMBER[9] parameters for zinc, integrating 5.0 nitrogen atoms and thus providing a stable $[Zn(Tf_2N)_5]^{3-}$ species with one bidentate and four monodentate $[Tf_2N]^-$ anions. This can also be observed from the correspondent Zn-$N(Tf_2N)$ RDF (Figure S1 R), which shows two distinct peaks: one of lower intensity related to the bidentate $[Tf_2N]^-$ and the more intense one provided by the four monodentate anions.

The average bond distance between Zn^{2+} and the first shell coordinating oxygen atoms shows a clear dependence from the employed potential. In particular, keeping constant the metal Lennard-Jones parameters, Zn-$O(Tf_2N)$ average distance decreases upon the RTIL force field following the KPL > MP > CL&P trend. This order has to be attributed to the different LJ parameters of the $[Tf_2N]^-$ oxygen atom in the force fields (Table S1), in particular σ, which becomes smaller following the same KPL

(3.46 Å) > MP (3.18 Å) > CL&P (2.96 Å) trend. On the other side, keeping constant the RTIL force field and changing Zn^{2+} LJ parameters, the average bond distance decreases following the SK > Merz > AMBER trend, even if the σ value for zinc decreases in a different order.

Table S2. MD results of Zn^{2+} first solvation shell structure in $[C_2mim][Tf_2N]$ and $[C_4mim][Tf_2N]$ employing all the tested Zn^{2+} Lennard-Jones parameters[7–9] and RTILs force fields.[2–6]

RTIL	RTIL force field	Zn^{2+} LJ parameters	$r_{Zn\text{-}O(Tf2N)}$ (Å)[a]	$n_{O(Tf2N)}$[b]	$n_{N(Tf2N)}$[c]
$[C_2mim][Tf_2N]$	CL&P	Merz	1.90	6.0	6.0
		SK	2.02	6.0	6.0
		AMBER	1.88	6.0	6.0
	KPL	Merz	2.00	6.0	6.0
		SK	2.14	6.0	6.0
		AMBER	1.98	6.0	6.0
$[C_4mim][Tf_2N]$	CL&P	Merz	1.88	6.0	6.0
		SK	2.00	6.0	6.0
		AMBER	1.86	6.0	6.0
	KPL	Merz	2.00	6.0	6.0
		SK	2.14	6.0	6.0
		AMBER	1.98	6.0	6.0
	MP	Merz	2.00	6.0	6.0
		SK	2.12	6.0	6.0
		AMBER	1.96	6.0	5.0

[a]Average bond distance between the Zn^{2+} ion and the coordinating oxygen atoms of the first solvation shell $[Tf_2N]^-$ anions; [b]Zn-O(Tf_2N) first RDF peak integration number; [c]Zn-N(Tf_2N) first RDF peak integration number.

1.2 Zn^{2+} solvation thermodynamics

Gibbs free energies of solvation of the Zn^{2+} ion in $[C_2mim][Tf_2N]$ and $[C_4mim]Tf_2N]$ have been calculated as described in the main text employing different RTILs force fields and LJ parameters for the metal ion and the results are reported in Table S3. The obtained values show that keeping constant the metal LJ parameters, ΔG_{solv} becomes more negative by changing the RTIL force field following the KPL < MP < CL&P trend. Since the $[Tf_2N]^-$ oxygen partial charge is the same in the tested force fields (-0.53 e, Table S1), it can be concluded that the more negative value obtained with CL&P is due to the smaller value of the LJ parameter σ, thus bringing to shorter Zn-O(Tf_2N) average distances

(Table S2) and stronger non-bonded interactions between the RTIL anion and the metal. On the other hand, for a given RTIL parameters set, the calculated ΔG_{solv} becomes more negative with the different Zn^{2+} LJ in the SK < Merz < AMBER order. Taking into account the calculated average Zn-O(Tf_2N) distances as a function of Zn^{2+} parameters (Table S2), this result confirms that the shorter the average distance (and as a consequence the stronger the non-bonded interaction), the more negative ΔG_{solv} results. Interestingly, the values obtained with the MP force field in combination with AMBER LJ parameters do not follow this trend. This exception should be attributed to the different $[Tf_2N]^-$ coordination towards zinc ($[Zn(Tf_2N)_5]^{3-}$ instead of $[Zn(Tf_2N)_6]^{4-}$) observed with this set of potentials (Table S2). As far as the absolute values are concerned, ΔG_{solv} is best reproduced in comparison with the experimental (Table 1 in the main text) with the CL&P force field in combination with Merz and AMBER parameters for zinc. On the other hand, KPL and MP force fields tend to underestimate ΔG_{solv} regardless of the employed LJ for zinc.

In order to obtain the ΔG_{trans}(water→RTIL), Zn^{2+} hydration free energies (ΔG_{hyd}) employing all the tested LJ parameters for the metal were also calculated. The resulting ΔG_{hyd} values reported in Table S4 are in agreement with that calculated by Merz *et al*.[7] in the parametrization of new LJ for Zn^{2+}.

CL&P gives also the best estimation of ΔG_{trans}(water→RTIL) (Table S3) in comparison with the experimental results, while the force fields by KPL and MP tend to overestimate it (too positive). Given that ΔG_{trans}(water→RTIL) reflects the tendency of Zn^{2+} to pass from an aqueous phase to the ionic liquid, the underestimation of the metal-RTIL interaction resulting with KPL and MP causes an equal overestimation of the free energy of transfer, as illustrated in Figure S2.

Taking into account these results, the combination of the CL&P force field for the RTILs and Merz *et al*. LJ parameters for Zn^{2+} have been evaluated to be the best compromise and employed for the rest of the work, as those giving the most accurate description for what concerns the thermodynamic part while providing a good representation of the structural features at the same time.

Zn-O

Zn-N

Zn-S

$[C_2mim][Tf_2N]$

A

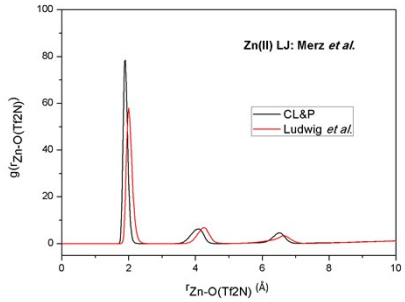

B

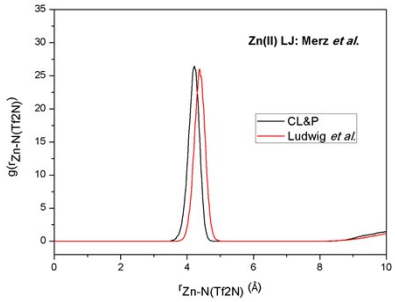

C

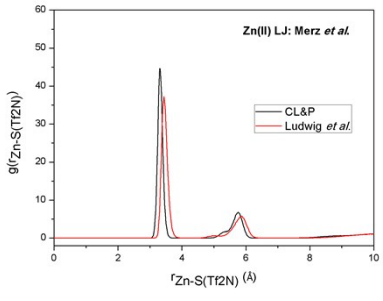

D

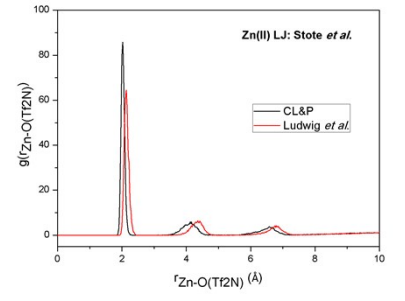

E

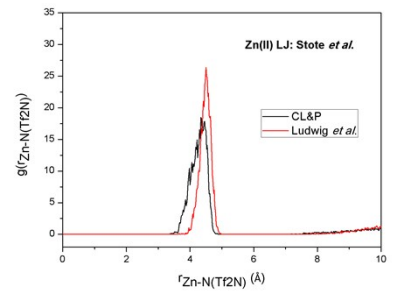

F

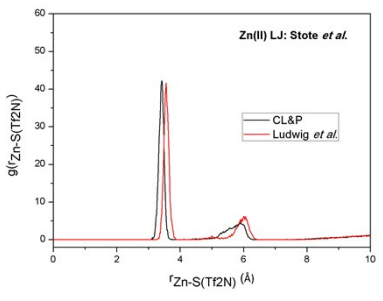

G

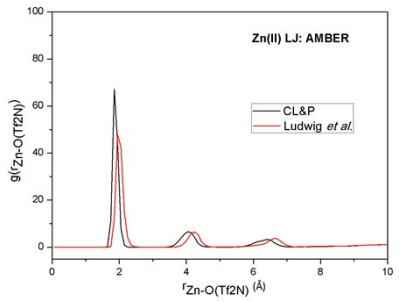

H

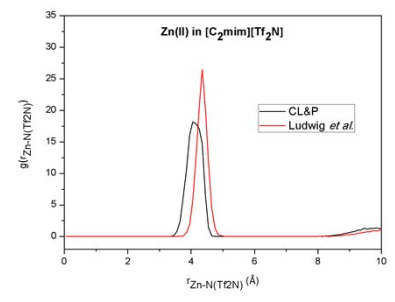

I

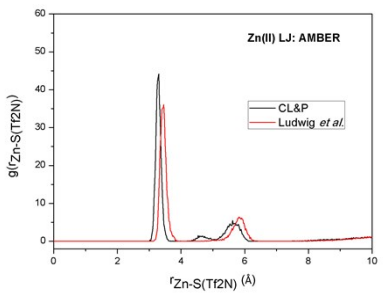

$[C_4mim][Tf_2N]$

J

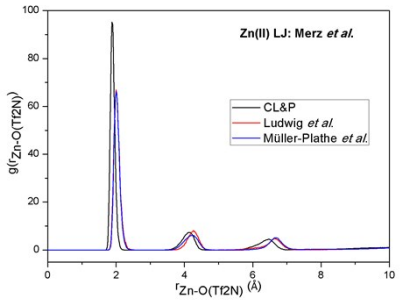

K

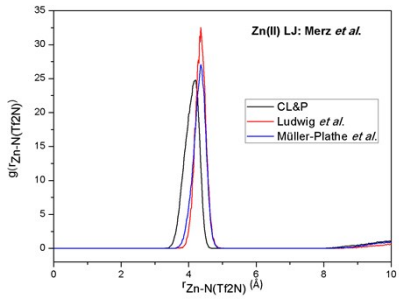

L

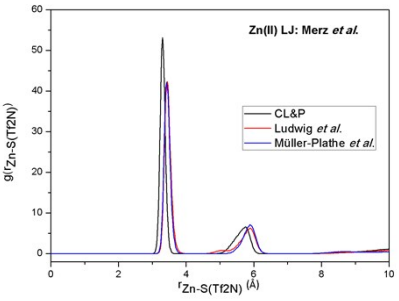

M

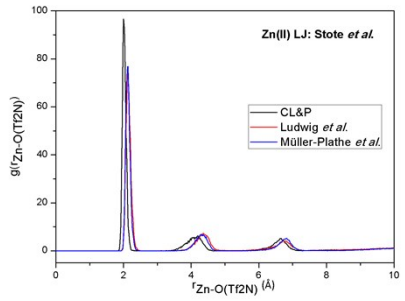

O

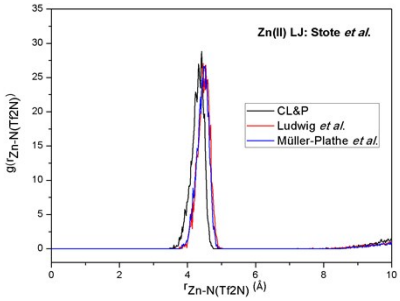

P

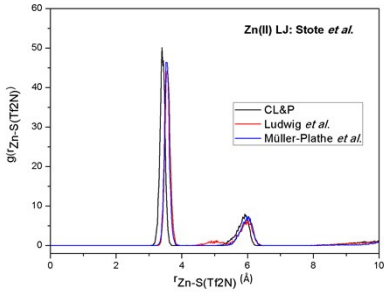

Q

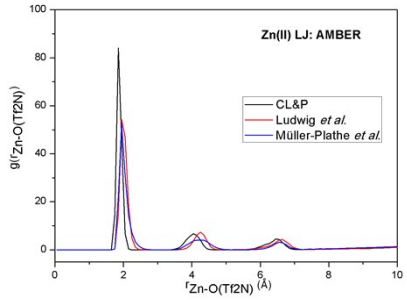

R

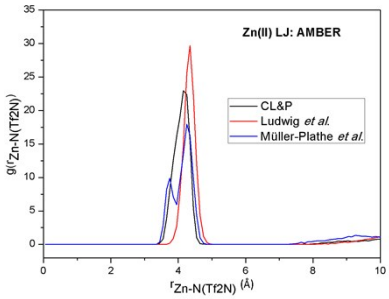

S

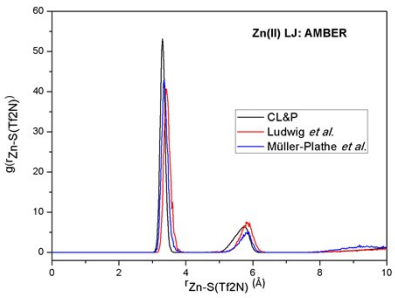

Figure S1. Zn-O(Tf_2N), Zn-N(Tf_2N) and Zn-S(Tf_2N) pairs radial distribution functions calculated for Zn^{2+} in [C_2mim]Tf_2N] and [C_4mim][Tf_2N] employing different Zn^{2+} Lennard-Jones parameters and RTILs force fields.

Table S3. Calculated Zn^{2+} Gibbs free energies of solvation ΔG_{solv} (kcal mol^{-1}) in [C_2mim][Tf_2N] and [C_4mim][Tf_2N] and free energies of transfer from water to the RTILs employing all the tested Zn^{2+} LJ parameters[7–9] and RTIL force fields.[2–6]

		Zn^{2+} LJ: Merz		Zn^{2+} LJ: SK		Zn^{2+} LJ: AMBER	
RTIL	RTIL force field	ΔG_{solv}[a]	ΔG_{trans} (water→RTIL)[b]	ΔG_{solv}[a]	ΔG_{trans} (water→RTIL)[b]	ΔG_{solv}[a]	ΔG_{trans} (water→RTIL)[b]
[C_2mim][Tf_2N]	CL&P	-437.7 ± 0.4	9.5 ± 0.5	-412.7 ± 1.1	1.6 ± 1.2	-452.4 ± 1.1	1.3 ± 1.3
	KPL	-397.6 ± 1.1	49.6 ± 1.2	-379.2 ± 0.6	35.1 ± 0.7	-397.7 ± 1.7	56.0 ± 1.9
[C_4mim][Tf_2N]	CL&P	-441.4 ± 0.3	5.8 ± 0.5	-415.5 ± 1.1	-0.2 ± 1.2	-454.7 ± 0.7	-0.9 ± 0.9
	KPL	-393.8 ± 0.9	53.4 ± 1.1	-375.0 ± 0.8	39.3 ± 0.9	-398.5 ± 0.7	55.2 ± 0.9
	MP	-413.3 ± 1.1	33.9 ± 1.3	-391.8 ± 1.4	22.4 ± 1.5	-402.9 ± 0.6	50.8 ± 0.8

[a]Zn^{2+} Gibbs free energy of solvation in RTILs; [b]Zn^{2+} Gibbs free energy of transfer from water to the RTILs calculated as ΔG_{trans}(water→RTIL) = ΔG_{solv}(g→RTIL) - ΔG_{hyd} with the ΔG_{hyd} values reported in Table S4.

Table S4. Calculated Zn^{2+} Gibbs free energy of hydration (ΔG_{hyd}, *kcal mol*$^{-1}$) with the LJ parameters[7–9] tested in this work.

Zn^{2+} LJ parameters	ΔG_{hyd}
Merz	-447.2 ± 0.2
SK	-414.3 ± 0.1
AMBER	-453.8 ± 0.2

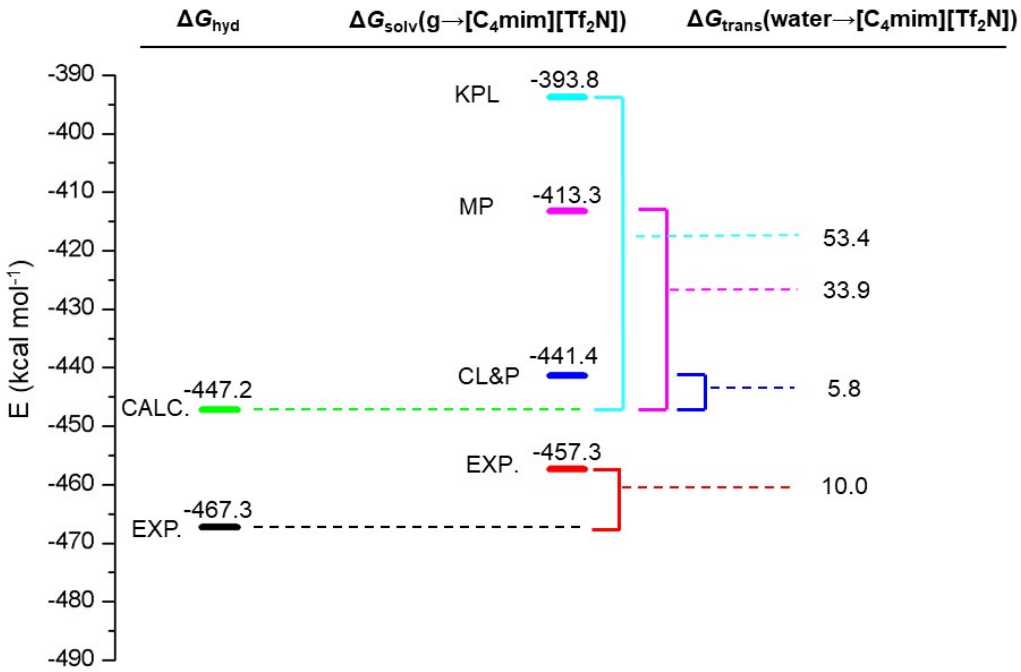

Figure S2. Diagram reporting Zn^{2+} experimental (values from Marcus,[14] black line) and calculated (green line) Gibbs hydration free energies within solvation free energies in $[C_4mim][Tf_2N]$ from literature experimental data[15–17] (red line) and calculated in this work with the tested force fields (blue: CL&P,[2–4] cyan: KPL;[5] purple: MP[6]). Differences between the solvation free energies in the RTIL and the correspondent hydration energy gives the free energies of transfer from water to $[C_4mim][Tf_2N]$. Only values obtained for Zn^{2+} represented with Merz LJ parameters[7] are showed.

Table S5. MD calculated densities (298.15 K, 1 atm) for the studied RTILs with the tested force fields within densities published by the authors in the original papers and experimental values. Data for water are also reported.

Solvent	Force field	Density (g ml^{-1})		
		This work	Authors	Exp.
[C_2mim][Tf_2N]	CL&P[2–4]	1.63	1.57	1.52[11]
	KPL[5]	1.55	Not given	
[C_4mim][Tf_2N]	CL&P[2–4]	1.54	1.48	1.44[11]
	KPL[5]	1.46	Not given	
	MP[6]	1.52	Not given	
Water	TIP3P[12]	0.992	0.982	0.997[13]

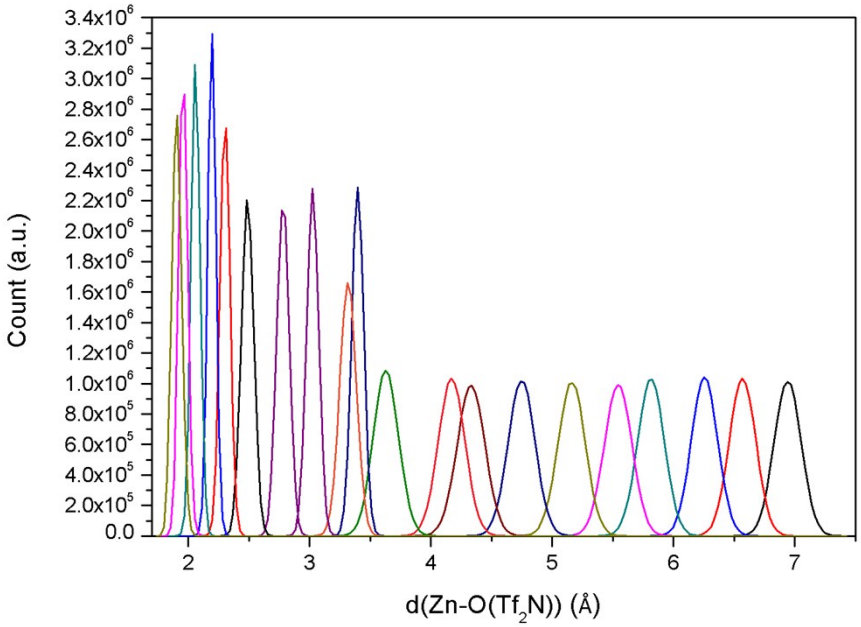

Figure S3. Histograms of the configurations within the umbrella sampling windows for the addition of a $[Tf_2N]^-$ anion to the $[Zn(Tf_2N)_5]^{3-}$ unit.

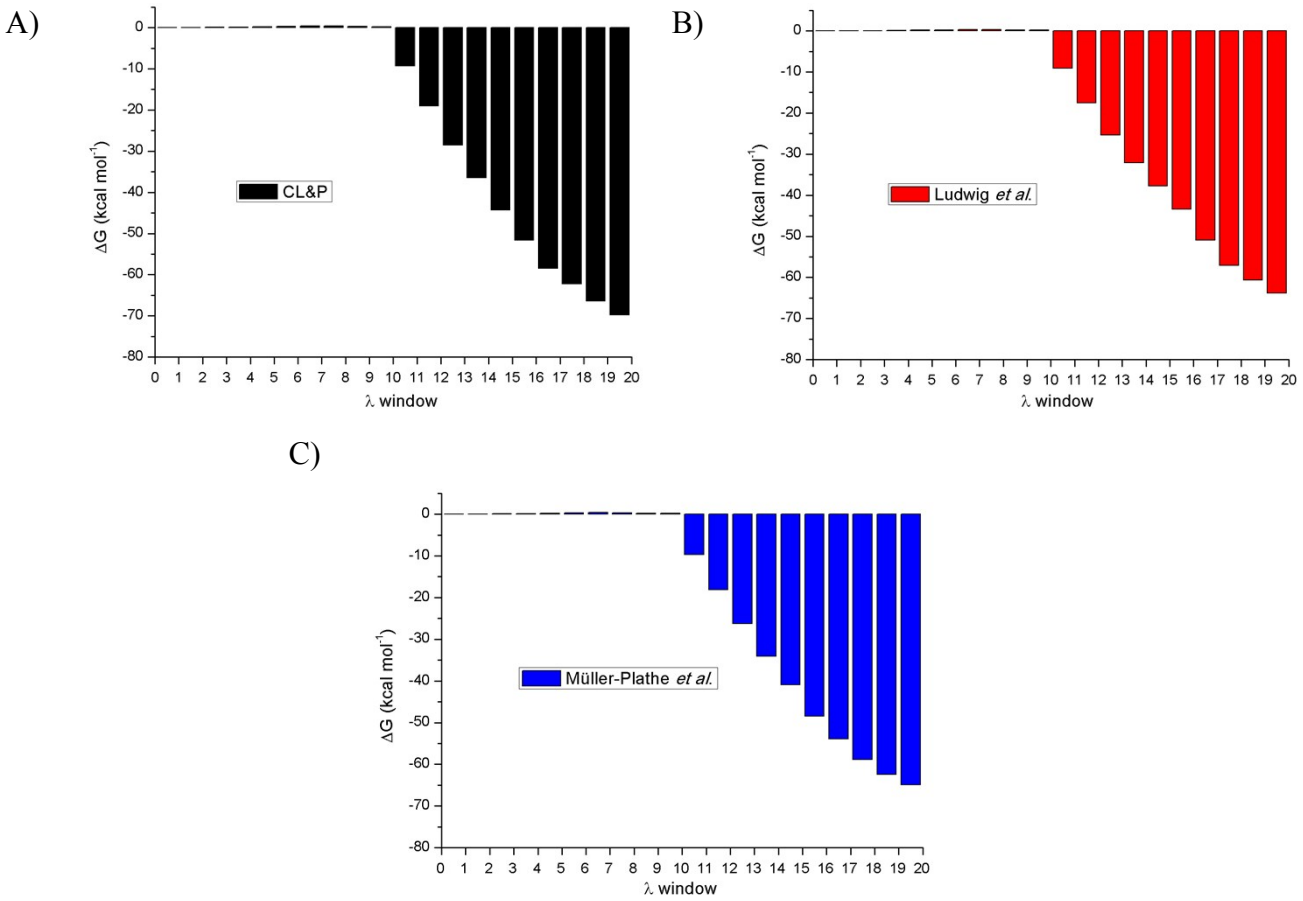

Figure S4. Gromacs BAR module output showing the relative free energy differences calculated between neighboring λ windows for Zn(II) represented with Merz *et al*. LJ parameters in [C_4mim][Tf_2N] with A) CL&P*;* B) Ludwig *et al*. and C) Müller-Plathe *et al*. force fields.

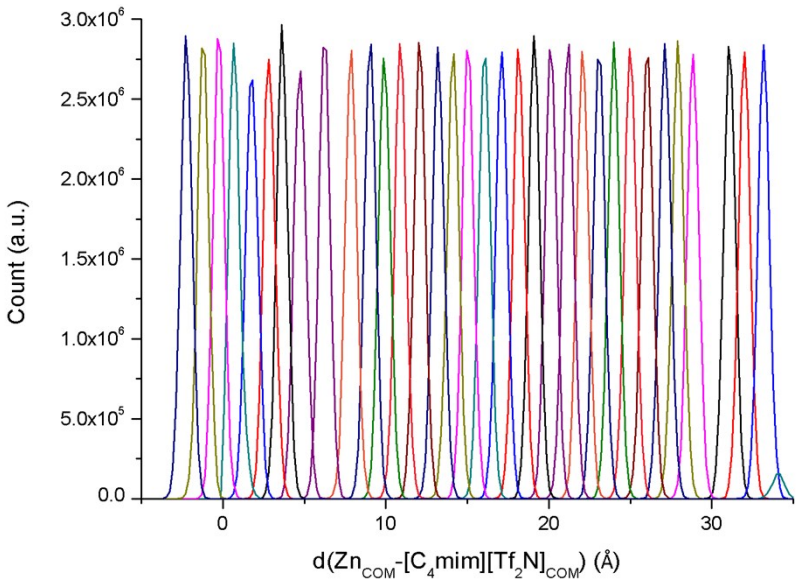

Figure S5. Histograms of the configurations within the umbrella sampling windows for the transfer of a Zn(II) ion from water to [C_4mim][Tf_2N] in a biphasic system.

A) B)

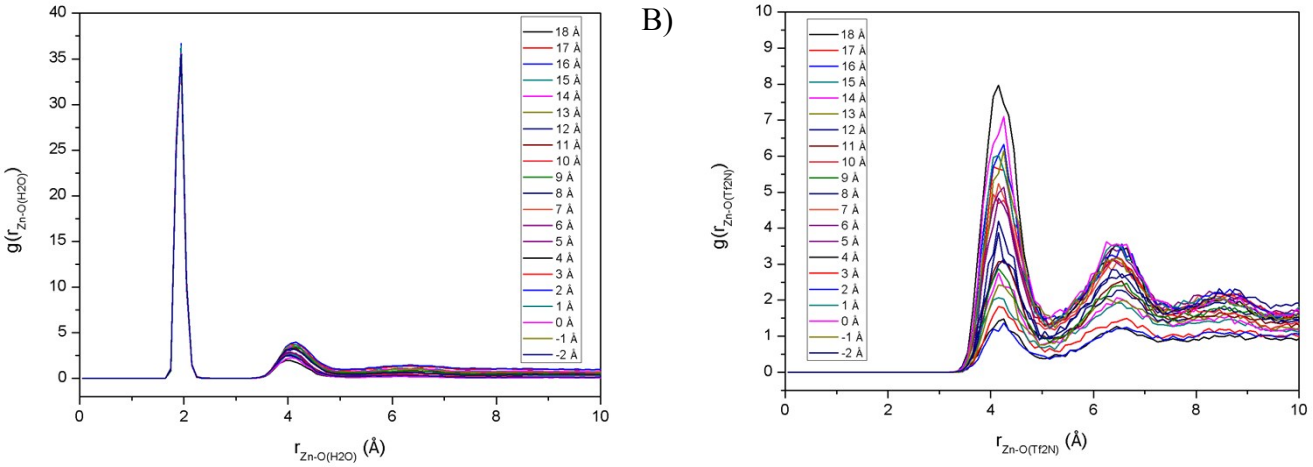

Figure S6. A) Zn-O(H_2O) and B) Zn-O(Tf_2N) pairs RDFs along the reaction coordinate between the interphase (d(Zn_{COM}-[C_4mim][Tf_2N]$_{COM}$) = 18 Å) and the ionic liquid bulk (d(Zn_{COM}-[C_4mim][Tf_2N]$_{COM}$) = -2 Å)

1 W. L. Maxwell, David S.; Tirado-Rives, Julian; Jorgensen, *J. Am. Chem. Soc.*, 1996, **118**, 11225–11236.

2 J. N. Canongia Lopes, A. A. H. Padua and J. Dechamps, *J. Phys. Chem. B*, 2004, **108**, 2038–2047.

3 J. N. Canongia Lopes, A. A. H. Padua and J. Dechamps, *J. Phys. Chem. B*, 2004, **108**, 11250.

4 J. N. Canongia Lopes and A. A. H. Padua, *J. Phys. Chem. B*, 2004, **108**, 16893–16898.

5 T. Köddermann, D. Paschek and R. Ludwig, *ChemPhysChem*, 2007, **8**, 2464–2470.

6 W. Zhao, E. Hossein, W. L. Cavalcanti and F. Müller-Plathe, *Z. Phys. Chem.*, 2007, **221**, 1549–1567.

7 P. Li, B. P. Roberts, D. K. Chakravorty and K. M. Merz, *J. Chem. Theory Comput.*, 2013, **9**, 2733–2748.

8 R. H. Stote and M. Karplus, *Proteins*, 1995, **23**, 12–31.

9 S. C. Hoops, K. W. Anderson and K. M. Merz, *J. Am. Chem. Soc.*, 1991, **113**, 8262–8270.

10 F. Sessa, V. Migliorati, A. Serva, A. Lapi, G. Aquilanti, G. Mancini and P. D'Angelo, *Phys. Chem. Chem. Phys.*, 2018, **20**, 2662–2675.

11 M. Krummen, P. Wasserscheid and J. Gmehling, *J. Chem. Eng. Data*, 2002, **47**, 1411–1417.

12 W. L. Jorgensen, J. Chandrasekhar, J. D. Madura, R. W. Impey and M. L. Klein, *J. Chem. Phys.*, 1983, **79**, 926.

13 N. K. ADAM, *Nature*, 1940, **146**, 145.

14 Y. Marcus, *J.Chem.Soc., Faraday Trans.*, 1991, **87**, 2995–2999.

15 A. Lewandowski and I. Stepniak, *Phys. Chem. Chem. Phys.*, 2003, **5**, 4215–4218.

16 S. Ahrland, *Pure Appl. Chem.*, 1982, **54**, 1451–1468.

17 Y. Marcus, *J. Chem. Soc., Faraday Trans.*, 1993, **89**, 713–718.